Electromagnetic dissociation of ^{59}Co, ^{89}Y, and ^{197}Au targets by relativistic heavy ions to $Z=26$

M. T. Mercier, John C. Hill, F. K. Wohn, C. M. McCullough, M. E. Nieland, J. A. Winger, C. B. Howard, S. Renwick, and D. K. Matheis
Ames Laboratory and Iowa State University, Ames, Iowa 50011

A. R. Smith
Lawrence Berkeley Laboratory, Berkeley, California 94720
(Received 20 November 1985)

The electromagnetic dissociation of ^{59}Co, ^{89}Y, and ^{197}Au target nuclei was inferred from measurements of cross sections for the one-neutron removal reaction. Beams of 2.1 GeV/nucleon ^{1}H, ^{12}C, and ^{20}Ne, 1.8 GeV/nucleon ^{40}Ar, and 1.7 GeV/nucleon ^{56}Fe projectiles were used. Beam intensities were monitored using the ^{12}C(RHI,X)^{11}C reaction, where RHI represents relativistic heavy ion beams. The experimental cross sections in excess of the estimated nuclear contributions are generally well described by use of the Weizsäcker-Williams method for calculating the electromagnetic dissociation contributions but increase more slowly as the projectile charge is increased. Cross sections for one-neutron removal reactions are large for the heavier projectiles, ranging up to 707 mb. For these cases a high percentage is from the electromagnetic dissociation process.

I. INTRODUCTION

Dissociation of relativistic heavy ions (RHI's) by the Coulomb fields of target nuclei, i.e., electromagnetic dissociation (ED), was first reported by Heckman and Lindstrom.[1] Evidence was seen for ED in both the single neutron and single proton channels for 2.1 GeV/nucleon ^{12}C and ^{16}O and 1.05 GeV/nucleon ^{12}C projectiles. Targets ranging from C to Pb were used with the largest ED effects observed for Ag and Pb. Subsequently ED was observed for 1.88 GeV/nucleon ^{56}Fe projectiles by Westfall *et al.*[2] using targets ranging from H to U. The elemental cross sections for the reaction X(^{56}Fe,Mn)Y were measured, where X represents various targets. Enhancement of the above cross section was noted for Ta, Pb, and U targets and attributed to ED effects on the one-proton out process. The U(^{56}Fe,Mn)Y cross section was measured to be 646±43 mb, but this value includes the sum of all processes of the type U(^{56}Fe,^{x}Mn)Y where $x \leq 55$ so the exact contribution of ED to the one-proton removal process was not clear.

Olsen *et al.*[3] observed ED in the fragmentation of 1.7 GeV/nucleon ^{18}O projectiles by targets ranging from Be to U. ED cross sections were measured for ^{17}O, ^{16}O, and ^{17}N projectilelike fragments which correspond to one-neutron, two-neutron, and one-proton out processes, respectively. The largest ED cross section was 140.8±4.1 mb for U(^{18}O,^{17}O)X.

ED in projectile fragmentation as reported in the above three experiments can be pictured as a purely electromagnetic process which occurs when RHI pass near a high-Z target nucleus but outside the range of the nuclear force. A virtual photon from the Coulomb field is absorbed by the projectile, resulting in the excitation, usually of a giant multipole resonance, which subsequently deexcites by particle emission. A similar process can occur in target nuclei where the roles of projectile and target are reversed. Figure 1 illustrates the two processes (one electromagnetic, one nuclear), which both lead to a target fragment which has lost a neutron. We reported in a recent Letter[4] the first experimental evidence for ED of target nuclei. Cross sections for the production of residues from ^{197}Au targets bombarded by various RHI Bevalac beams were measured. The ED cross sections observed for heavy pro-

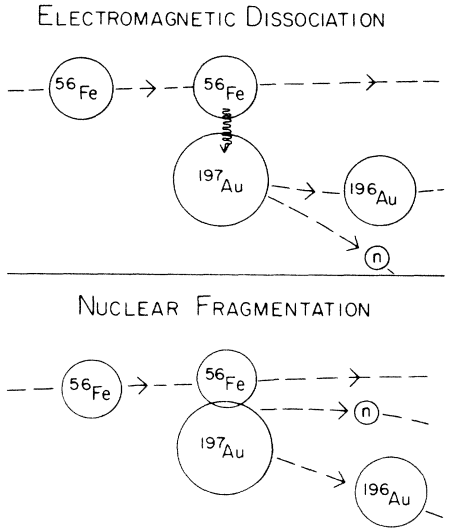

FIG. 1. Diagram illustrating the competing processes of electromagnetic dissociation (ED) and nuclear fragmentation, both resulting in the loss of one neutron from the target nucleus during the ^{197}Au(^{56}Fe,X)^{196}Au reaction. ED, which is an electromagnetic process, can occur over a large range of impact parameters, but nuclear fragmentation is limited by the short range of the nuclear force.

jectiles were quite large, but the errors were also large due to the unavailability at the time of suitable monitor cross sections for the ^{40}Ar and ^{56}Fe beam intensities. Subsequently, measurement of the ^{12}C(^{56}Fe,X)^{11}C monitor cross section[5] was carried out. We report in this paper details of our ED experiments for Co and Y as well as Au targets. This work was reported earlier[6] in preliminary form.

II. CALCULATION OF ELECTROMAGNETIC DISSOCIATION CROSS SECTIONS

In order to calculate cross sections for the ED process one must first form the product of the virtual photon spectrum $N_\gamma(E_\gamma)$ with that of the appropriate photonuclear cross section $\sigma_\gamma(E_\gamma)$. This process is indicated for the ^{197}Au(^{56}Fe,X)^{196}Au reaction in Fig. 2. In order to get the ED cross section σ_{ED} we integrate the above product:

$$\sigma_{ED}=\int_0^\infty N_\gamma(E_\gamma)\sigma_\gamma(E_\gamma)dE_\gamma \ .$$

In our calculations $\sigma_\gamma(E_\gamma)$ was obtained from the National Bureau of Standards (NBS) Digital DATA Library.[7]

Two methods that have been used[1-4] for calculating $N_\gamma(E_\gamma)$ are the Weizsäcker-Williams (WW) method for virtual photons,[8] which assumes a point charge, and the method of Jäckle and Pilkuhn (JP),[9] which assumes a Yukawa charge distribution. In the case of projectile fragmentation the JP method is quite insensitive to the charge distribution of the target. In this case the results using a Gaussian charge distribution and those using a point charge were the same within the error of the measured photonuclear cross sections. (See for example Fig. 3 in Ref. 3.) Unfortunately the difference in the JP and WW calculations for a point charge differ by about 30%. Our experiment is not very sensitive to the shape of the photon spectrum. The effect of this difference is to shift the free parameter b_{min}, which is the minimum impact parameter for the ED process. Unfortunately the difference in the WW and JP results correspond to a change in b_{min} of about 3 fm. A thorough discussion of these problems is given in Ref. 3.

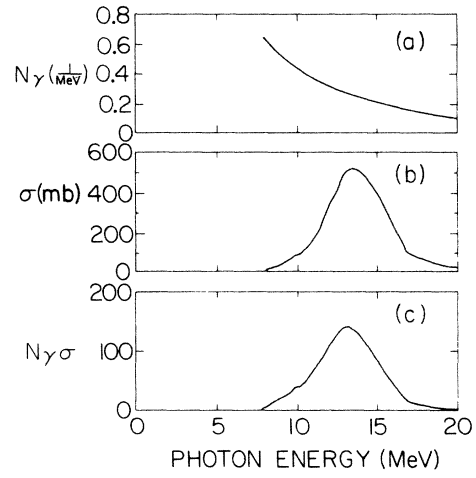

FIG. 2. Components necessary for calculation of the electromagnetic dissociation cross section σ_{ED}. (a) shows the virtual-photon spectrum N_γ for 1.7 GeV/nucleon ^{56}Fe projectiles calculated using the Weizsäcker-Williams method from Ref. 8. (b) shows the ^{197}Au(γ,n)^{196}Au photonuclear cross section taken from Ref. 7. (c) shows the product of (a) and (b) that is integrated to obtain σ_{ED}.

Many of the WW calculations[1-4] of virtual photon spectra used in the analysis of the ED effect have assumed straightline trajectories for the projectile and ignored contributions due to multipoles other than $E1$. Goldberg[10] has determined the virtual photon spectrum for RHI's on stationary targets for all multipoles in terms of the classical trajectories of the ions. The $E1$ multipole was dominant. The effects of a curved projectile trajectory were considered[10] for projectile $Z/A=0.5$ and $\gamma=1.25$ ($\sim$235 MeV/nucleon). The difference between the resulting virtual-photon spectrum and that from a straightline trajectory (Jackson value[8]) was small and decreased by a factor of 2 if $\gamma=1.5$ ($\sim$470 MeV/nucleon). For our experiments $\gamma\simeq3.0$ was typical, thus the straightline trajectory approximation was accurate. As pointed out by Goldberg[10] the difference between the straightline approximation and the curved projectile trajectory is due almost entirely to the difference in the minimum impact parameter required to give the correct distance of closest approach. It is thus possible to account for both the extended charge distribution of the projectile and the curved nature of the projectile trajectory by slightly rescaling the minimum impact parameter b_{min}.

Contributions to ED from $M1$ transitions are expected to be negligible,[10] but the contribution from $E2$ can be significant, since for $\gamma=3$ the $E2$ virtual photon spectrum exceeds that for $E1$ by about a factor of 3. Both Goldberg[10] and Winther and Alder[11] have carried out calculations of the contribution of $E2$ transitions to the ED effect. Goldberg found that for $\gamma=3$ the ratio of $E2$ to $E1$ strengths was 9% for ^{238}U projectiles on a ^{238}U target. A similar estimate for our cases indicates an $E2$ contribution of less than 7%. The relative $E2$ strength decreases with increasing projectile energy due to the decreased $E2$ strength relative to $E1$ in the virtual photon spectra. Bertulani and Baur[12] have calculated virtual photon spectra for various multipoles using the plane-wave Born approximation. There results are very similar to those obtained by Goldberg.[10]

III. EXPERIMENTAL METHOD

A. Irradiation and counting procedures

The bombardments were carried out in the external beam at the Lawrence Berkeley Laboratory (LBL) Bevalac accelerator, using beams of 2.1 GeV/nucleon p, ^{12}C, and ^{20}Ne, 1.8 GeV/nucleon ^{40}Ar, and 1.7 GeV/nucleon ^{56}Fe projectiles. The targets consisted of foils of the monoisotopic elements Co, Y, and Au. Each target foil was placed between an Al foil (0.038 mm thick) on the upstream side and a Mylar foil (0.13 mm thick) on the downstream side. The Al foils were used to obtain a beam profile by counting ^{24}Na and the Mylar served as a rigid

backing for the target. Three different thicknesses of each target foil were bombarded simultaneously in order to obtain corrections for secondary reactions which are significant for one-neutron removal processes.

In a typical bombardment a target string was irradiated in a short run of one to ten minutes to obtain a good beam calibration from a 0.159 cm polystyrene target using the ^{12}C(RHI,X)^{11}C reaction. The thin polystyrene was positioned first in the target string to minimize the production of ^{11}C from secondary products produced in the other targets. Next in the string came three metal targets of the same thicknesses as those used for the main run. The last target in the string was a thick 5.08 cm polystyrene block in which the long-lived (53.3 d) ^{7}Be activity could be accurately measured and compared to ^{11}C activity in the thin upstream polystyrene target. This procedure, repeated for each RHI-target combination, enabled us to transfer the ^{11}C beam calibration function to thick-target ^{7}Be activity, thus providing a suitable absolute beam monitor for the much longer main experimental runs. The last element was an ion chamber which was used to compare total beam on target during the short and long runs and measure fluctuations in beam intensity that must be used to make corrections to the yield calculations.

Next a longer run lasting from 1 to 12 h was carried out using a new target string, but with identical target parameters. In this run the metal targets were positioned first in the string in order to minimize secondary reactions in the metal. The metal targets increased in thickness as one went downstream and were each separated by 25 cm to minimize secondary reactions produced by cross talk between targets. The different thicknesses were used to correct for secondary reactions within the target, as discussed below. Typical thicknesses of the various metal targets are given in Table I.

The beam intensities were measured by counting ^{11}C produced in the ^{12}C(RHI,X)^{11}C reaction on polystyrene targets using a well-calibrated NaI(Tl) γ spectrometer described in Ref. 13. Accurate cross sections for the ^{12}C(RHI,X)^{11}C monitor reactions were determined in a series of separate experiments.[5,13] Values used in the present work for these cross sections are given in Table II. The cross sections for 2.1 GeV/nucleon ^{12}C and 1.7 GeV/nucleon ^{56}Fe projectiles have been directly measured using procedures discussed in Ref. 13. The ^{12}C(^{20}Ne,X)^{11}C cross section was assumed to be the same as the measured value at 1.05 GeV/nucleon,[5] since no information is available at 2.1 GeV/nucleon. This assumption is true for ^{12}C projectiles[13] to within a few percent, and the uncertainty for ^{20}Ne projectiles in Table II has been correspondingly increased. No measurement has been made of the ^{12}C(^{40}Ar,X)^{11}C cross section for RHI's. We thus interpolated between the ^{12}C, ^{20}Ne, and ^{56}Fe projectile cross sections to obtain a value for the ^{12}C(^{40}Ar,X)^{11}C cross section.

TABLE I. Typical targets and thicknesses.

Target	Thickness (mg/cm^2)
^{59}Co[a]	50,120,230
^{89}Y[b]	50,90,180
^{197}Au[a]	50,90,240

[a]Foils obtained commercially with maximum total metallic impurities of a few parts per million.
[b]Foils produced at the Ames Laboratory with maximum total metallic impurities of a few parts per million.

TABLE II. Monitor cross sections used in determining beam intensities in this work.

Projectile	Energy (GeV/nucleon)	σ (mb) ^{12}C(RHI,X)^{11}C	^{27}Al(p,3pn)^{24}Na
p	2.1	27.7±1.0[a]	
p	28		7.92±0.18[b]
^{12}C	2.1	60.9±0.6[c]	
^{20}Ne	1.05	80.4±1.4[d]	
^{40}Ar	1.8	92.0±3.0[e]	
^{56}Fe	1.7	99.6±0.9[f]	

[a]See Refs. 14–18 and text.
[b]See Ref. 18.
[c]See Ref. 13.
[d]Value based on measurement of ^{12}C(^{20}Ne,X)^{11}C cross section using 1.05 GeV/nucleon ^{20}Ne projectiles. See Refs. 5, 13, and text.
[e]Value based on interpolation between ^{12}C(^{12}C,X)^{11}C, ^{12}C(^{20}Ne,X)^{11}C, and ^{12}C(^{56}Fe,X)^{11}C cross sections.
[f]See Ref. 5.

Using techniques similar to those employed for measuring the ^{12}C(^{12}C,X)^{11}C cross section, the ^{12}C(p,pn)^{11}C cross section was measured[14] to be 27.7±0.3 mb at 3.65 GeV. This is essentially consistent with an old value[15] of 26.2±0.9 mb measured at 2 GeV. It is well known[16] that the ^{12}C(p,pn)^{11}C cross section is approximately constant between 0.6 and 6 GeV. The absolute values of the (p,pn) cross sections have been thrown in doubt by recent measurements[17,18] at 0.8 GeV giving values of 32.0±1.0 and 30.1±1.1 mb, respectively. We use a value of 27.7±1.0 mb for the ^{12}C(p,pn)^{11}C cross section at 2.1 GeV. Our results could be normalized if more accurate measurements were made in the future at 2.1 GeV.

As is discussed below, it was necessary to measure (p,X) cross section for all targets at proton energies higher than those available at the Bevalac. We thus irradiated Co, Y, and Au metal targets similar to those described above in the 28-GeV proton beam of the alternating-gradient synchrotron (AGS) accelerator at Brookhaven. Irradiations lasted for about one minute and 8 mg/cm^2 Al foils were used to monitor the beam intensity using the ^{27}Al(p,3pn)^{24}Na reaction.[18]

In both the Bevalac and AGS runs all metal targets were shipped by air to the Ames Laboratory at Iowa State University for counting of the appropriate residual γ-ray activities using two low-energy photon spectrometer (LEPS) and two Ge(Li) detectors. The counting continued for periods as long as one year and the detectors were calibrated for absolute efficiency using NBS standard sources. Counting dead time corrections were made using a standard 60 Hz pulser. The γ-ray information was collected in four, 4096-channel spectra. The decay of isotopes was

followed in most cases for several half-lives and corrections for interfering activities were made. The above decay curves were fit using known half-lives and the appropriate yields were calculated. Yields were always determined from the thinnest target to minimize corrections due to secondary particles. Information on beam intensity and target geometry was used to obtain cross sections for the reactions of interest. A number of corrections were necessary.

B. Corrections and error analysis

A large number of sources of systematic error were considered in the analysis of the data. Fluctuations of the RHI beam intensity were monitored using the output of an ion chamber which was fed into a digital current integrator whose output was summed and periodically recorded by computer. Corrections of yield for beam intensity fluctuations were negligible for most products of interest with long half-lives counted in Ames, but were of considerable importance in counting the ^{11}C used as a monitor of the beam intensity.

All targets were mounted on a 0.13 mm Mylar backing. It was determined by counting several of the Mylar backings after irradiation that loss of reaction products out of the target due to recoil was negligible. This was due to the fact that relatively thick targets were used, and that targetlike fragments receive a relatively small amount of kinetic energy in RHI reactions.

Systematic errors can arise due to finite spread and nonuniformity of the beam intensity and variations in thickness of the target. In several targets, circles 0.64 cm in diameter were punched and weighed on an analytical balance. In a typical test about 16 circles gave a total spread of less than 5% over the face of a 5.1 by 5.1 cm target. The finite spread of the beam on the target was determined by counting the ^{24}Na activity in a 0.038 mm Al foil on the upstream side of each of the targets. After irradiation the Al foil was cut into a 1.3-cm diameter central circle and three concentric rings of successively 2.5, 3.8, and 5.1 cm in outer diameter and counted. The information obtained was used to correct results from counting of γ rays using Ge detectors. Details of these corrections are described below.

The Ge(Li) and LEPS detectors used at Ames to determine the yield of various radioactive nuclides by γ counting were calibrated for energy and absolute efficiency using NBS standards. The detectors were calibrated as a function of distance of the source from the detector face. Due to the relatively large size of the beam spot during some runs, coupled with weak activities, it was necessary to count at the face of the detector. It was also necessary to calibrate the detectors as a function of source position in a direction parallel to the detector face. This correction was particularly important for low-energy γ rays. Yields were then corrected using information on the spread of the beam obtained from the Al foils. Corrections were also made for self-absorption of γ rays in the targets.

Yields were determined when possible by averaging over those obtained from several strong γ rays from the same isotope. In some cases the independent yield was obtained whereas in others only the cumulative yield could be measured. For the one-neutron removal process of interest, corrections were made in some cases due to feeding from a parent produced purely by secondary reactions.

In a few cases it was necessary to make corrections for geometry-dependent coincidence summing. This effect can either lower or raise the apparent yield of a particular γ ray depending on the circumstances. Though generally small, the largest correction for a particularly unfavorable case was 46%. The coincidence summing corrections were only necessary for runs with ^{12}C and ^{56}Fe projectiles where the beam intensities were low requiring counting on the face of a large volume Ge(Li) detector. In order to make the above correction, total efficiencies of our detectors were determined for the γ-ray energy range from 122 to 1836 keV using ^{57}Co, ^{203}Hg, ^{113}Sn, ^{85}Sr, ^{54}Mn, ^{65}Zn, and ^{88}Y sources.

Generally the most significant corrections were those for production of a nuclide due to secondary reactions in the target. For deep spallation products these corrections were negligible, but for the one-neutron removal products (mass close to that of target nucleus) the correction was typically of the order of 10%. In each case three targets of successively larger thicknesses were simultaneously ir-

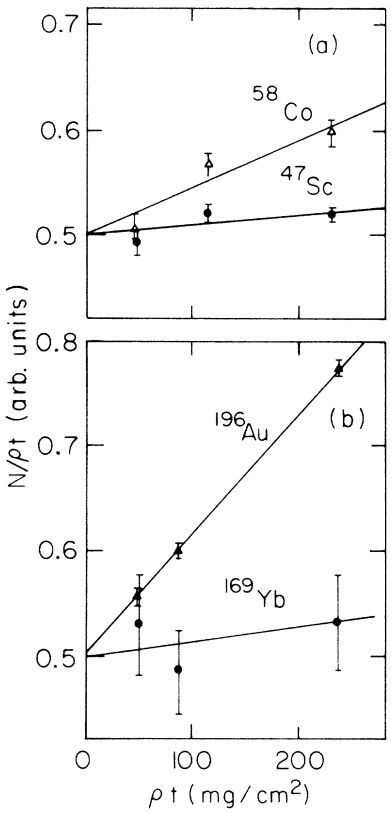

FIG. 3. Typical plots of information used to correct for production of various nuclides by secondary particles produced in the target. (a) shows results for typical products from 2.1 GeV/nucleon ^{20}Ne projectiles on ^{59}Co targets and (b) shows results for the same projectiles on ^{197}Au targets. The corrections for the one-neutron removal products are substantial.

radiated. Secondary production from targetlike fragments due to cross talk between the targets was negligible due to the fact that targets were separated by a distance of 25 cm. We estimate the ratio of secondary production from the adjacent target to be less than 1% of that due to secondary production within the target itself. We thus neglect cross talk in the consideration of the secondary correction. Secondary production in the first target from projectilelike fragments was assumed to be negligible. This is valid due to the fact that less than 1% of the RHI beam is absorbed in any of our target stacks. Also, projectilelike fragments with Z and A near to that of the target are expected to have cross sections for production of targetlike fragments similar to those for the primary beam particles.

For correction due to secondary particles absorbed by the same target in which they were produced, we assume $N(t)=at+bt^2$ where a and b are constants, and $N(t)$ gives the amount of activity produced as a function of target thickness t. Parameter b would be 0 if secondary processes were negligible. $N(t)$ is measured for the three targets. In Fig. 3(a) an example is shown using data from ^{20}Ne projectiles on ^{59}Co leading to the fragments ^{58}Co and ^{47}Sc. In Fig. 3(b) similar plots are shown for ^{20}Ne projectiles on a ^{197}Au target leading to the fragments ^{196}Au and ^{169}Yb. The constants a and b are determined by a weighted least squares fit. Next the fraction S of the product produced by secondary reactions is determined. Finally the saturation activity for the thinnest target is multiplied by $(1-S)$ to correct for secondary production of the nuclide of interest. In the example given above the secondary correction for ^{196}Au in the thinnest target is 7.2% while that for ^{169}Yb in the same target is only 1.2%.

C. Determination of cross sections

The experimental cross sections were determined from the expression

$$\sigma(\text{cm}^2)=\frac{N(\text{atoms/sec})M(\text{g/mole})}{f(\text{proj/sec})\rho(\text{g/cm}^2)N_a(\text{atoms/mole})} .$$

The target density ρ was determined by weighing our 5.1 by 5.1 cm targets on an analytical balance, and the total beam flux f was determined from the ^{11}C measurements. N, the disintegration rate at saturation, was determined from the γ-ray count rate by

$$N\left[\frac{\text{atoms}}{\text{sec}}\right]=\frac{n\left[\frac{\text{counts}}{\text{sec}}\right]}{\lambda\epsilon bGB} .$$

n refers to counts per second at saturation and ϵ, b, G, and B represent absolute detector efficiency, γ-ray branching ratio, γ-ray absorption in the target, and correction for finite width of the irradiated spot, respectively. The counting rate was measured as a function of time for several half-lives in most cases and the decay curve was fit using half-lives from the literature in order to determine the activity at the end of irradiation and thus the saturation activity n. In what follows the term one-neutron removal refers to processes in which one neutron but no protons are removed from the target nucleus.

IV. ONE-NEUTRON REMOVAL CROSS SECTIONS

A. ^{59}Co(RHI,X)^{58}Co

The independent yield of ^{58}Co ($T_{1/2}=70.82$ d) (Ref. 19) was determined by following the decay of the 811-keV γ ray which is 99.5% abundant.[19] Both ^{58}Ni and ^{58}Fe are stable. The experimental cross sections for the ^{59}Co(RHI,X)^{58}Co reactions, along with corrections due to secondary reactions, are given in Table III.

B. ^{89}Y(RHI,X)^{88}Y

The independent yield of ^{88}Y ($T_{1/2}=106.6$ d) (Ref. 20) was determined by measuring the decay of the 898- and 1836-keV γ rays which are, respectively, 94.0% and 99.4% abundant.[20] Although ^{88}Sr is stable, ^{88}Zr ($T_{1/2}=83.4$ d) (Ref. 20) is produced by secondary reactions and the corrections are small but not negligible. They were determined by measuring the yield of ^{88}Zr by following the decay of the 394-keV γ ray and correcting the decay curve for ^{88}Y. The corrections were at most a few percent (3% for ^{20}Ne). The experimental cross sections for the ^{89}Y(RHI,X)^{88}Y reactions are given in Table IV.

C. ^{197}Au(RHI,X)^{196}Au

The independent yield of ^{196}Au ($T_{1/2}=6.183$ d) (Ref. 21) was determined by measuring the decay of the 333- and 355-keV γ rays which are 22.9% and 86.9% abundant,[21] respectively. Both ^{196}Hg and ^{196}Pt are stable. The yield also included that for all isomers of ^{196}Au. The correction for ^{196}Au^m ($T_{1/2}=9.7$ h) (Ref. 21) is small due

TABLE III. Cross sections for one-neutron removal reactions by RHI on Co targets.

Projectile	Energy (GeV/nucleon)	Total RHI Beam intensity (particles)	Cross section (mb) ^{59}Co(RHI,X)^{58}Co	% correction secondary reactions
p	2.1	1.0×10^{14}	46±3	1.3
p	28	3.0×10^{14}	39±2	1.4
^{12}C	2.1	1.8×10^{11}	89±5	7
^{20}Ne	2.1	2.0×10^{12}	132±7	4
^{56}Fe	1.7	5.3×10^{10}	194±9	5

TABLE IV. Cross sections for one-neutron removal reactions by RHI on Y targets.

Projectile	Energy (GeV/nucleon)	Total RHI Beam intensity (particles)	Cross section (mb) ^{89}Y(RHI,X)^{88}Y	% correction secondary reactions
p	2.1	9.8×10^{13}	51±4	7
p	28	3.5×10^{14}	49±3	3
^{12}C	2.1	1.6×10^{11}	115±6	10
^{20}Ne	2.1	2.1×10^{12}	160±7	6
^{40}Ar	1.8	5.7×10^{11}	283±11	3
^{56}Fe	1.7	1.7×10^{11}	353±14	4

to its short half-life compared to ^{196}Au and its low yield in RHI reactions.[22] The experimental cross sections for the ^{197}Au(RHI,X)^{196}Au reactions are given in Table V.

V. NUCLEAR CONTRIBUTION TO FEW NEUTRON REMOVAL CROSS SECTIONS

A. Factorization and limiting fragmentation

In order to estimate the nuclear contribution to the total cross section we make use of the concept of factorization[23] of the nuclear cross section. This assumes $\sigma^F_{TP}=\gamma^F_T\gamma^T_P$, where F, T, and P indicate dependencies on target fragment, target, and projectile, respectively. This notation is similar to that of Heckman and Lindstrom[1] but with the roles of P and T reversed. Factorization implies that the yield of a particular fragment from the target due to nuclear interactions will be independent of the beam except through the geometric factor γ^T_P. Thus, for example, the ratio

$$\sigma[^{197}\mathrm{Au}(^{20}\mathrm{Ne},X)F_i]/\sigma[^{197}\mathrm{Au}(\mathrm{p},X)F_i]$$

should have a constant value $\gamma^{\mathrm{Au}}_{\mathrm{Ne}}/\gamma^{\mathrm{Au}}_{\mathrm{p}}$ for any fragment F_i. We also make use of the hypothesis of limiting fragmentation introduced by Benecke *et al.*[24] which states that for sufficiently high projectile energies the cross section for production of the fragment F_i is independent of energy.

The concept of factorization has been tested for target fragmentation of Au nuclei by Kaufman *et al.*[25] using 4.8 and 25 GeV ^{12}C and 7.6 GeV ^{20}Ne projectiles. Cross sections for fragments ranging in A from 24 to 196 were measured. Cole and Porile[26] also tested factorization in the fragment mass range from $A=24$ to 52 on a series of six targets (Cu, Ag, Gd, Ta, Au, and U). In addition to the work of Cole and Porile on low mass targets, Porile *et al.*[27] have tested factorization by measuring the ratio of target fragment cross sections for 25.2 GeV ^{12}C and 300 GeV protons incident on Ag targets. Finally, factorization for target fragmentation of Cu targets has been tested in a series of experiments using 28-GeV protons, 25-GeV ^{12}C, and 80-GeV ^{40}Ar projectiles.[28]

One conclusion from the above studies was that cross sections for heavy ion induced reactions should be compared with proton cross sections of comparable total kinetic energy. For ^{197}Au factorization was found to be approximately true[25] in the mass region from $A=70$ to 190, but deviations from exact factorization such as a shallow minimum in the σ(RHI)/σ(p) ratio was noted at about $A=140$. An enhancement of σ(RHI)/σ(p) for $A<40$ was observed[25] which can be attributed to the effects of central collisions resulting in the enhanced production of light fragments for RHI. In the low mass region, studies of Cu and Ag spallation[26–28] are relevant to our studies of Co and Y spallation. Cumming *et al.*[28] determined σ(RHI)/σ(p) for 80-GeV ^{40}Ar and 28-GeV p on Cu targets to be essentially constant in the A range from 20 to 60. ^{7}Be fragments were enhanced for ^{40}Ar projectiles due to central collisions. Similar results were obtained[28] for 2.1 GeV/nucleon ^{12}C projectiles. Porile *et al.*[27] obtained similar results by using Ag targets and determining σ(RHI)/σ(p) for 25.2 GeV ^{12}C and 300 GeV protons. They noted a significant enhancement in σ(RHI)/σ(p) for $A<30$, again due to the effects of central collisions.

The concept of limiting fragmentation has been thoroughly studied for Au target fragmentation by Kaufman and co-workers.[22,25,29] They found that although the formation cross section for ^{196}Au by protons was essen-

TABLE V. Cross sections for one-neutron removal reactions by RHI on Au targets.

Projectile	Energy (GeV/nucleon)	Total RHI Beam intensity (particles)	Cross section (mb) ^{197}Au(RHI,X)^{196}Au	% correction secondary reactions
p	2.1	7.7×10^{13}	66±5	8
p	28	2.8×10^{14}	62±4	7
^{12}C	2.1	1.6×10^{11}	178±7	5
^{20}Ne	2.1	9.2×10^{11}	268±11	7
^{40}Ar	1.8	6.2×10^{11}	463±30	5
^{56}Fe	1.7	2.2×10^{11}	707±52	5

tially independent of energy above 200 MeV, limiting fragmentation applied[22,29] for deep spallation products only after the proton energy was higher than 10 GeV. The similarity in the shape of the σ(RHI)/σ(p) curves for 4.8 GeV and 25 GeV ^{12}C projectiles[25] gives one confidence that limiting fragmentation is approximately valid for 2.1 GeV/nucleon ^{12}C, at least in the range $60 < A < 190$. We thus assume limiting fragmentation to be a valid concept for RHI used in this experiment.

We estimate the nuclear part of the one-neutron removal channel from ratios such as

$$\sigma[^{197}\text{Au(RHI},X)F_i]/\sigma[^{197}\text{Au(p},X)F_i]$$

as a function of the fragment mass. Since the limiting fragmentation region for protons is not reached for deep spallation products at least until 10 GeV, as discussed above, we used the proton cross sections measured by us at 28 GeV which are consistent with the measurements by Kaufman *et al.*[29] at 11.5 and 300 GeV. If we assume, for example, factorization for the nuclear part of the ^{197}Au(RHI,X)^{196}Au cross section, then

$$\sigma_{\text{nuc}}(\text{RHI},^{196}\text{Au}) = \left[\frac{\sigma(\text{RHI},F_i)}{\sigma(\text{p},F_i)}\right]_{\text{ave}} \sigma(\text{p},^{196}\text{Au}) ,$$

where the fragments used in the average have masses A in the range $60 < A < 190$.

B. Results for nuclear contribution to one-neutron removal cross sections

1. *Co targets*

The ratio $\sigma[^{59}\text{Co(RHI},X)F_i]/\sigma[^{59}\text{Co(p},X)F_i]$ is plotted in Fig. 4 for ^{56}Fe and ^{20}Ne projectiles. A similar plot was constructed for ^{12}C projectiles. The cross section ratios were determined for 13 fragments in the mass range from ^{24}Na to ^{58}Co. For some projectiles not all 13 ratios could be determined due to low beam intensities. As can be seen in Fig. 4, factorization is valid in the mass range from $A=43$ to 52 for all projectiles. ^{24}Na fragments are enhanced for RHI due to central collisions and ^{58}Co due to ED. We also expect some enhancement of the ^{57}Co cross section due to ED effects.

For ^{12}C and ^{20}Ne projectiles factorization appears to be valid in the mass range from ^{43}K to ^{56}Co, therefore for those projectiles the ratio

$$\sigma[^{59}\text{Co(RHI},X)F_i]/\sigma[^{59}\text{Co(p},X)F_i]$$

was determined from a weighted average of the individual fragment ratios with A between 43 and 56. The results

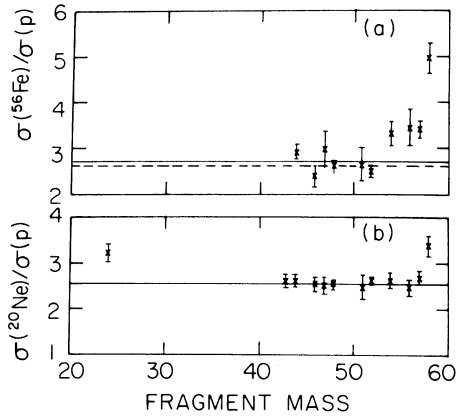

FIG. 4. The experimentally determined ratio $\sigma[^{59}\text{Co(RHI},X)F_i]/\sigma[^{59}\text{Co(p},X)F_i]$ for (a) 1.7 GeV/nucleon ^{56}Fe and (b) 2.1 GeV/nucleon ^{20}Ne projectiles. The solid horizontal lines indicate the weighted averages for the above ratios using eight points ranging from $^{44}\text{Sc}^{m}$ to ^{56}Co for ^{56}Fe and ten points ranging from ^{43}K to ^{56}Co for ^{20}Ne projectiles. The dashed line in (a) indicates a different average obtained if the points for ^{54}Mn and ^{56}Co are excluded.

along with an estimate of the "nuclear" cross section for production of ^{58}Co are given in Table VI. The uncertainty of the above ratio includes both statistical factors, uncertainties due to the deviation of the data from strict factorization, and uncertainties in the ^{11}C monitor cross sections.

The data for ^{56}Fe projectiles required special consideration. In Fig. 4(a) it is clear that the points for ^{57}Co, ^{56}Co, and ^{54}Mn are anomalously high. This could be due to ED effects for ^{57}Co but is rather puzzling for ^{56}Co and ^{54}Mn. ^{54}Mn can be produced by emission of one neutron plus an α particle from the ^{59}Co target and ^{56}Co is produced by emission of three neutrons from ^{59}Co. ED processes could enhance both processes although we would not expect this to occur for ^{56}Co. The target, excited by ED, could emit an α particle due to the relatively low Coulomb barrier for ^{59}Co. Measurements to be carried out in the future using ^{139}La projectiles may provide information on this problem. The ratio

$$\sigma[^{59}\text{Co}(^{56}\text{Fe},X)F_i]/\sigma[^{59}\text{Co(p},X)F_i]$$

was determined using both the ^{54}Mn and ^{56}Co points for consistency. A value of 2.71 ± 0.19 was obtained. If the above two points had been excluded the value for the ratio would be 2.63 ± 0.14. Both values are shown in Fig. 4(a).

TABLE VI. Nuclear cross sections for one-neutron out products from Co targets.

RHI	Number of ratios	Ratio mass range (A)	$\left\{\frac{\sigma[^{59}\text{Co(RHI},X)F_i]}{\sigma[^{59}\text{Co(p},X)F_i]}\right\}_{\text{ave}}$	Nuclear cross section $\sigma[^{59}\text{Co(RHI},X)^{58}\text{Co}]$ (mb)
^{12}C	9	44–56	2.13 ± 0.13	83 ± 7
^{20}Ne	10	43–56	2.57 ± 0.17	100 ± 8
^{56}Fe	8	44–56	2.71 ± 0.19	106 ± 10

2. Y targets

The ratio $\sigma[^{89}Y(RHI,X)F_i]/\sigma[^{89}Y(p,X)F_i]$ is plotted in Fig. 5 for ^{56}Fe and ^{20}Ne projectiles. Similar plots were constructed for ^{12}C and ^{40}Ar projectiles. The cross section ratios were determined for up to 20 fragments in the mass range from ^{24}Na to ^{88}Y. Factorization is approximately valid in the mass range from $A=43$ to 86. Both ^{24}Na and ^{28}Mg are enhanced by central collisions for RHI. The one-neutron out product ^{88}Y is also enhanced. Just below $A=50$ some increase in the ratio is seen. This represents a small violation of factorization. Similar small violations were observed[26,27] for Ag targets. It is interesting to note that the enhancement of products near the target mass seen in the $^{59}Co(^{56}Fe,X)F_i$ reaction was not observed for the $^{89}Y(^{56}Fe,X)F_i$ reaction.

The ratio $\sigma[^{89}Y(RHI,X)F_i]/\sigma[^{89}Y(p,X)F_i]$ was determined as described above for Co targets. The mass range used was $A=44$ to 86. The results along with an estimate for the nuclear cross section for the $^{89}Y(RHI,X)^{88}Y$ reaction are given in Table VII.

3. Au targets

The ratio $\sigma[^{197}Au(RHI,X)F_i]/\sigma[^{197}Au(p,X)F_i]$ is plotted in Fig. 6 for ^{56}Fe and ^{20}Ne projectiles. Similar plots were constructed for ^{12}C and ^{40}Ar projectiles. The cross section ratios were determined for 22 fragments in the mass range from ^{24}Na to ^{196}Au. Not all ratios were measured for all beams due to weak activities in some cases. Figure 6 shows that factorization is approximately valid between $A=80$ and 190. A trace of structure similar to that seen by other observers[22,25,29] is seen in our work in that the above ratio has a shallow minimum at approximately $A=140$. The ^{24}Na points are enhanced for RHI's due to central collisions and the ^{196}Au ratio is strongly enhanced due to ED.

The ratio $\sigma[^{197}Au(RHI,X)F_i]/\sigma[^{197}Au(p,X)F_i]$ was determined as described above for Co and Y targets. The mass range used was $A=83$–190. The results along with an estimate of the nuclear cross section for the $^{197}Au(RHI,X)^{196}Au$ reaction are given in Table VIII.

VI. ELECTROMAGNETIC DISSOCIATION CROSS SECTIONS FOR ONE-NEUTRON REMOVAL PROCESSES

A. The calculated cross section

The Weizsäcker-Williams method for virtual photons[8] was used to calculate the electromagnetic-dissociation

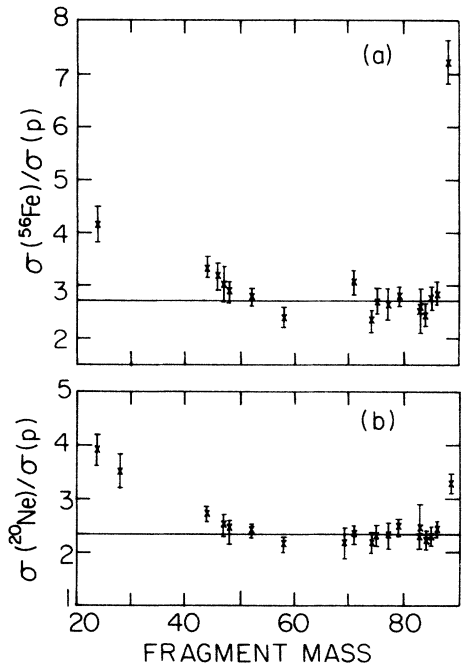

FIG. 5. The experimentally determined ratio $\sigma[^{89}Y(RHI,X)F_i]/\sigma[^{89}Y(p,X)F_i]$ for (a) 1.7 GeV/nucleon ^{56}Fe and (b) 2.1 GeV/nucleon ^{20}Ne projectiles. The horizontal lines indicate the weighted averages for the above ratios using 16 points from $^{44}Sc^m$ to ^{86}Y for ^{56}Fe and 17 points from $^{44}Sc^m$ to ^{86}Y for ^{20}Ne projectiles.

portion of the appropriate one-neutron removal cross sections using a modification of a computer code of Cook.[30] The procedure and its limitations have been discussed in Sec. II of this paper. The only adjustable parameter in the calculation is the minimum impact parameter b_{min}. Rather than letting it vary arbitrarily we have chosen it to be of the form

$$b_c = r_0[A_p^{1/3}+A_t^{1/3}-X(A_p^{-1/3}+A_t^{-1/3})]$$

suggested by Vary,[31] where the A's refer to the projectile and target, respectively. b_c can be visualized as a radius characterizing the range of the short-range nuclear force. Outside of this range nuclear processes are assumed to be very unlikely whereas for impact parameters less than b_c nuclear interactions are assumed to dominate. We thus used b_c as a lower limit for the ED process.

In the expression for b_c, the term $r_0(A_p^{1/3}+A_t^{1/3})$ can be thought of as a "touching radius" for the two nuclei. The term $X(A_p^{-1/3}+A_t^{-1/3})$ is a curvature correction. It

TABLE VII. Nuclear cross sections for one-neutron out products from Y targets.

RHI	Number of ratios	Ratio mass range (A)	$\left\{\frac{\sigma[^{89}Y(RHI,X)F_i]}{\sigma[^{89}Y(p,X)F_i]}\right\}_{ave}$	Nuclear cross section $\sigma[^{89}Y(RHI,X)^{88}Y]$ (mb)
^{12}C	14	44–86	2.14±0.16	106±10
^{20}Ne	17	44–86	2.36±0.16	117±10
^{40}Ar	16	44–86	3.04±0.22	151±13
^{56}Fe	16	44–86	2.75±0.23	136±14

TABLE VIII. Nuclear cross sections for one-neutron out products from Au targets.

RHI	Number of ratios	Ratio mass range (A)	$\left\{\frac{\sigma[^{197}\text{Au(RHI},X)F_i]}{\sigma[^{197}\text{Au(p},X)F_i]}\right\}_{\text{ave}}$	Nuclear cross section $\sigma[^{197}\text{Au(RHI},X)^{196}\text{Au}]$ (mb)
^{12}C	11	87–181	1.66±0.17	103±12
^{20}Ne	18	83–190	1.86±0.21	115±14
^{40}Ar	17	83–188	1.85±0.22	115±15
^{56}Fe	11	83–181	1.71±0.21	106±14

TABLE IX. ED cross sections for the ^{59}Co(RHI,X)^{58}Co reaction.

RHI	Energy (GeV/nucleon)	Total σ (mb)	Nuclear σ[a] (mb)	Measured ED σ[b] (mb)	Calculated ED σ (mb)
p	2.1	46±3			0.3
^{12}C	2.1	89±5	83±7	6±9	8.7
^{20}Ne	2.1	132±7	100±8	32±11	23
^{56}Fe	1.7	194±9	106±10	88±14	122

[a]Nuclear cross sections based on a measured value of 39±2 mb for the ^{59}Co(p,X)^{58}Co reaction using 28-GeV protons.
[b]Measured ED cross section assumed to be zero for protons.

TABLE X. ED cross sections for the ^{89}Y(RHI,X)^{88}Y reaction.

RHI	Energy (GeV/nucleon)	Total σ (mb)	Nuclear σ[a] (mb)	Measured ED σ[b] (mb)	Calculated ED σ (mb)
p	2.1	51±4			0.6
^{12}C	2.1	115±6	106±10	9±12	17
^{20}Ne	2.1	160±7	117±10	43±12	46
^{40}Ar	1.8	283±11	151±13	132±17	128
^{56}Fe	1.7	353±14	136±14	217±20	248

[a]Nuclear cross sections based on a measured value of 49±3 mb for the ^{89}Y(p,X)^{88}Y reaction using 28-GeV protons.
[b]Measured ED cross section assumed to be zero for protons.

TABLE XI. ED cross sections for the ^{197}Au(RHI,X)^{196}Au reaction.

RHI	Energy (GeV/nucleon)	Total σ (mb)	Nuclear σ[a] (mb)	Measured ED σ[b] (mb)	Calculated ED σ (mb)
p	2.1	66±5			1.5
^{12}C	2.1	178±7	103±12	75±14	45
^{20}Ne	2.1	268±11	115±14	153±18	121
^{40}Ar	1.8	463±30	115±15	348±34	346
^{56}Fe	1.7	707±52	106±14	601±54	678

[a]Nuclear cross sections based on a measured value of 62±4 mb for the ^{197}Au(p,X)^{196}Au reaction using 28-GeV protons.
[b]Measured ED cross section assumed to be zero for protons.

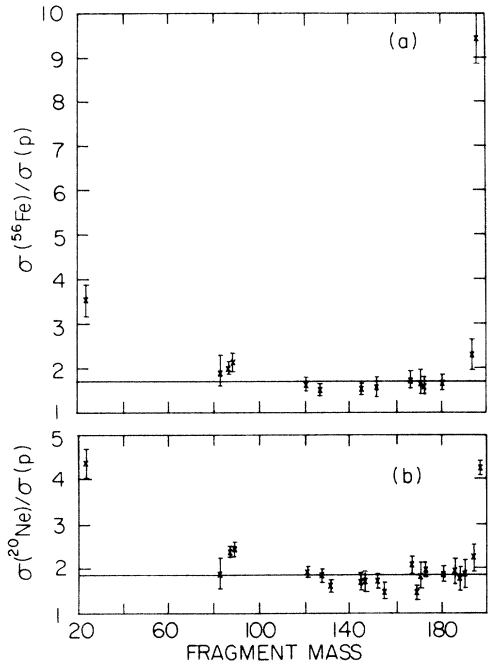

FIG. 6. The experimentally determined ratio $\sigma[^{197}\text{Au(RHI},X)F_i]/\sigma[^{197}\text{Au(p},X)F_i]$ for (a) 1.7 GeV/nucleon ^{56}Fe and (b) 2.1 GeV/nucleon ^{20}Ne projectiles. The horizontal lines indicate the weighted averages for the above ratios using 11 points from ^{83}Sr to ^{181}Re for ^{56}Fe and 18 points from ^{83}Sr to ^{190}Ir for ^{20}Ne projectiles.

can be pictured[31] as a term necessary to maintain a fixed mean number of nucleon-nucleon collisions as either A_p or A_t increases. The constants r_0 and X were determined[31] to be 1.34 fm and 0.75, respectively. The functional form of b_c is suggested from Glauber theory[32] and the values for r_0 and X were from fits[31] to nucleon-nucleus and nucleus-nucleus calculations from Ref. 33

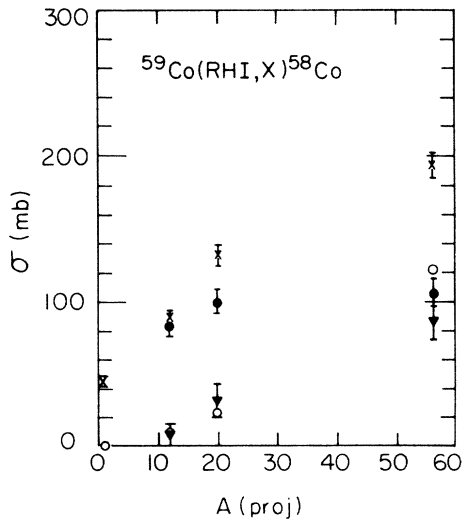

FIG. 7. Various cross sections for the ^{59}Co(RHI,X)^{58}Co reaction as a function of projectile mass. The cross sections are total measured (×'s), empirical nuclear (filled circles), calculated ED (open circles), and measured ED (filled triangles).

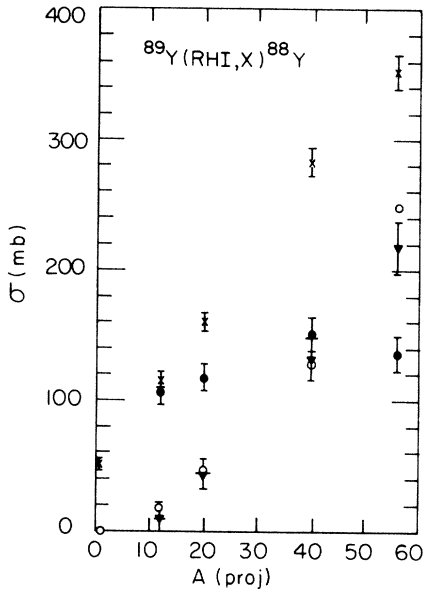

FIG. 8. Various cross sections for the ^{89}Y(RHI,X)^{88}Y reaction as a function of projectile mass. The cross sections are total measured (×'s), empirical nuclear (filled circles), calculated ED (open circles), and measured ED (filled triangles).

and densities from electron scattering data.[34] The results of the ED calculations are given above in Tables IX–XI.

B. Estimate of measured ED cross section

We define the "measured" ED cross section to be the one-neutron removal cross section measured in this exper-

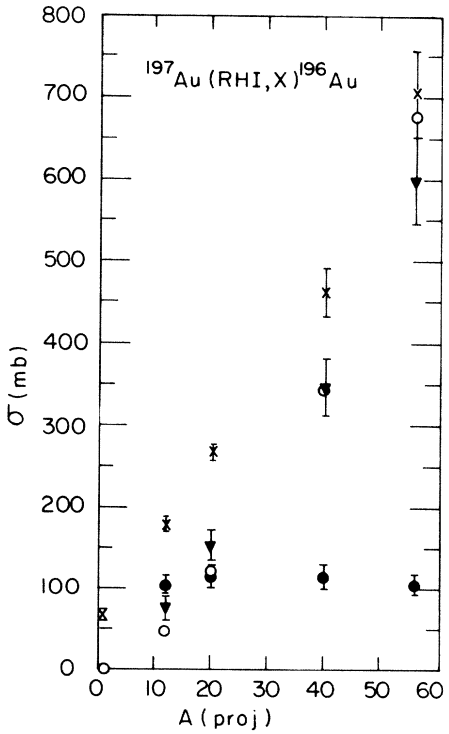

FIG. 9. Various cross sections for the ^{197}Au(RHI,X)^{196}Au reaction as a function of projectile mass. The cross sections are total measured (×'s), empirical nuclear (filled circles), calculated ED (open circles), and measured ED (filled triangles).

iment minus the empirically determined nuclear cross section for the one-neutron removal process described in Sec. V. The results are given in Tables IX–XI for ^{59}Co, ^{89}Y, and ^{197}Au targets, respectively. The total measured cross section, empirically derived nuclear cross section, calculated ED cross section, and the measured ED cross section for one-neutron out processes in ^{59}Co, ^{89}Y, and ^{197}Au are plotted as a function of projectile mass in Figs. 7–9, respectively. Uncertainties associated with the total measured cross sections and the empirically derived nuclear cross sections are discussed above. The uncertainties for the measured ED cross sections include uncertainties from both the total and nuclear cross sections.

VII. DISCUSSION

To summarize, we report here the observation of electromagnetic dissociation in target fragmentation of light (^{59}Co), medium (^{89}Y), and heavy (^{197}Au) nuclei by relativistic heavy ions. The effect was observed for the reaction in which one neutron was removed from the target nucleus. Preliminary results have been reported earlier.[4,6] The ED effect can be seen to increase both with the Z of the projectile and the Z of the target (see Figs. 7–9). It becomes quite large (601±54 mb) for the ^{197}Au(^{56}Fe,X)^{196}Au reaction.

The one-neutron removal cross sections can be described by an empirically determined nuclear part which uses the concept of factorization plus an ED part which uses a virtual photon spectrum determined by the Weizsäcker-Williams (WW) method folded in with the appropriate measured photonuclear (γ,n) cross section. Good agreement is generally observed between the calculated and measured ED cross sections but the calculated value is higher than the measured results for the heaviest projectile (^{56}Fe) by typically about 10%. It is not clear whether this discrepancy is "real" but measurements planned using 1.3 GeV/nucleon ^{139}La projectiles will help to illuminate this problem. We calculate the ^{197}Au(^{139}La,X)^{196}Au cross section to be 2.6 b.

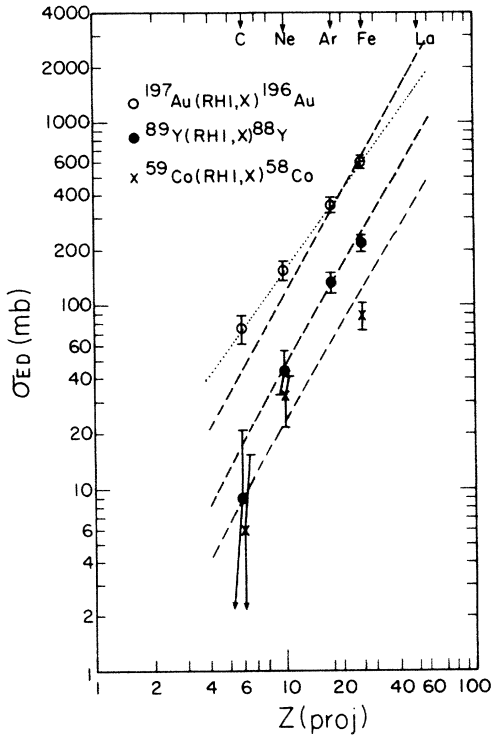

FIG. 10. Data points are experimental ED cross sections and dashed lines connect the WW calculations of Tables IX–XI (or Figs. 7–9). The dotted line, an empirical fit to the Au data, is discussed in the text.

Figure 10 summarizes the ED cross sections for the target fragmentation cases reported here. Use of a log-log plot of σ_{ED} versus the projectile charge Z_p makes the WW calculations nearly linear. To an accuracy of ~2%, all three dashed WW lines in Fig. 10 follow a simple power law of the form $\sigma=\sigma_1 Z_p^b$ with the same slope b of 1.80.

Three features of the systematic behavior of the ED cross sections are apparent from Fig. 10. First, the WW calculation is successful in that the main dependences on target and projectile are reproduced reasonably well using the simple relationship (see Sec. VI A) for the minimum impact parameter b_c. Second, the WW calculation overestimates the ED cross section for the heaviest projectile, ^{56}Fe. These two features were noted above.

Third, as Fig. 10 reveals, the WW calculation predicts a more rapid increase of σ_{ED} with increasing projectile charge than does the data. This can be readily seen for the four Au data points, which lie on a straight line, but one with a slope b significantly less than 1.80. If these four points are used to empirically determine an ED cross section of the form $\sigma=\sigma_1 Z_p^b$, then the empirical parameters are $\sigma_1=5.64$ mb and $b=1.43$. The rms deviation between the four data points and the fit is only 3.0 mb, indicating a nearly perfect fit. (The dotted line in Fig. 10 shows how colinear the four Au points are.)

Although the Y and Co data points in Fig. 10 are reasonably well fit by the lines of slope 1.80, the slope of 1.43 also provides a good fit and is clearly better for Co and Y points with large Z_p. The larger Z_p points provide a more reliable measure of σ_{ED} since the experimentally deduced σ_{ED} for the low Z_p points have large systematic uncertainties due to the nuclear part of the total cross section being much larger than σ_{ED} when Z_p and A_t are small. The differences between slopes of 1.80 and 1.43 can be significant. As mentioned above, the reaction ^{197}Au(^{139}La,X)^{196}Au, with $Z_p=57$, has a WW estimate of 2.6 b for σ_{ED}. Extrapolating the empirical fit of slope 1.43 gives a prediction of 1.8 b. Measurement with ^{139}La RHI's should clearly distinguish between these two predictions.

A number of mechanisms can be postulated to explain the diminished ED cross sections for the highest Z projectiles. Among these are interference between Coulomb and nuclear processes, interference between one- and two-photon emission, and depletion of large fragments due to more catastrophic collisions using heavy projectiles. Additional data provided by higher projectile charges will be needed in order to test the adequacy of the WW technique for calculating σ_{ED} and assess the importance of the above processes.

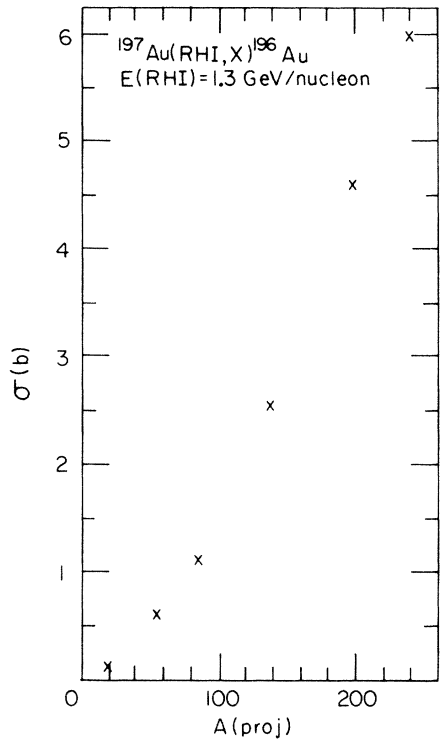

FIG. 11. Calculated values of the ED cross section for the ^{197}Au(RHI,X)^{196}Au reaction at a typical Bevalac energy of 1.3 GeV/nucleon using the WW formalism. Points given are for ^{20}Ne, ^{56}Fe, ^{86}Kr, ^{139}La, ^{197}Au, and ^{238}U projectiles.

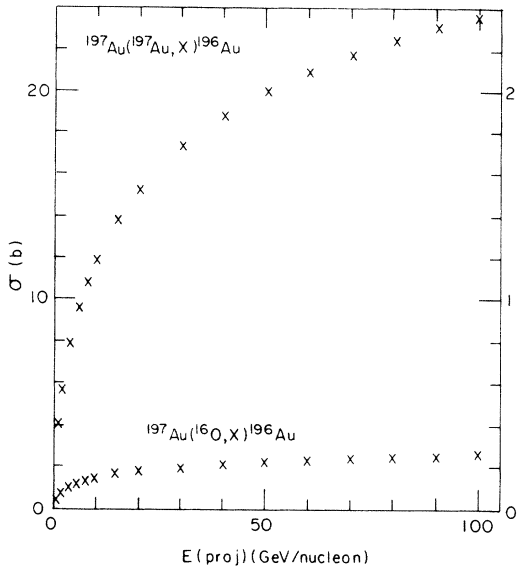

FIG. 12. Calculated values of the ED cross section for the ^{197}Au(^{197}Au,X)^{196}Au reaction with projectile energies ranging up to 100 GeV/nucleon. A stationary target is assumed. The lower curve gives the ED cross section for the ^{197}Au(^{16}O,X)^{196}Au reaction. The $\sigma(b)$ scale for the (^{16}O,X) reaction is to the right of the figure.

In this paper we have determined the ED cross section for the one-neutron removal process only. It would be of interest to determine the ED cross section for one-proton removal. This cross section would be small but measurable for low-Z targets. Unfortunately for our targets, the one-proton out residual nucleus is β stable. We have measured the yield of residual nuclei resulting from the two-neutron out reaction. The ED effects are small but measurable in some cases. The two-neutron out ED results will be reported in a future publication.

Calculations using the WW method indicate that ED cross sections can become very large for large Z projectiles at ultrarelativistic energies. If such large cross sections do indeed exist, they might be a constraint[35] on the storage times for very relativistic heavy ion colliding-beam accelerators and should also be considered in the planning of experiments for the above facilities. We have extended our WW calculations to predict the ^{197}Au(RHI,X)^{196}Au ED cross sections for the highest Z projectiles presently available at the Bevalac. We have chosen an energy of 1.3 GeV/nucleon for all projectiles. The results are shown in Fig. 11. The ED cross section rises to 6 b for the ^{197}Au(^{238}U,X)^{196}Au reaction. We expect the nuclear part of the ^{197}Au(^{238}U,X)^{196}Au cross section to be no more than a few hundred mb. The maximum energy for ^{238}U ions at the Bevalac is about 1.0 GeV/nucleon which gives a calculated ED cross section for the above process of 5.3 b.

It is also of interest to estimate the increase in the ED cross section for a representative heavy projectile as a function of energy. We have thus calculated the ED cross section for the ^{197}Au(^{197}Au,X)^{196}Au reaction on a stationary target as a function of projectile energy up to 100 GeV/nucleon. The results are shown in Fig. 12. The ED cross section rises to 23.8 b at 100 GeV/nucleon. For colliding beams the cross section would be correspondingly higher. We also show in Fig. 12 the results for the ^{197}Au(^{16}O,X)^{196}Au reaction up to 100 GeV/nucleon. Using beams of 50 and 200 GeV/nucleon that will soon become available at CERN it should thus be possible to test the energy dependence of the WW procedure for ED reactions at ultrarelativistic energies.

ACKNOWLEDGMENTS

The authors thank B. C. Cook for the use of his WW computer code and M. R. Clover for modifications made to the code. Interesting conversations with J. P. Vary are acknowledged. We also thank Y. Y. Chu for help with irradiations at the AGS accelerator. Special thanks go to Fred Lothrop and the Bevalac staff for their help.

[1]H. H. Heckman and P. J. Lindstrom, Phys. Rev. Lett. **37**, 56 (1976).
[2]G. D. Westfall, L. W. Wilson, P. J. Lindstrom, H. J. Crawford, D. E. Greiner, and H. H. Heckman, Phys. Rev. C **19**, 1309 (1979).
[3]D. L. Olsen, B. L. Berman, D. E. Greiner, H. H. Heckman, P. J. Lindstrom, G. D. Westfall, and H. J. Crawford, Phys. Rev. C **24**, 1529 (1981).
[4]M. T. Mercier, J. C. Hill, F. K. Wohn, and A. R. Smith, Phys. Rev. Lett. **52**, 898 (1984).
[5]J. C. Hill, J. A. Winger, C. M. McCullough, A. R. Smith, J. B. McCaslin, and P. J. Karol, Phys. Rev. C **33**, 557 (1986).
[6]J. C. Hill, M. T. Mercier, F. K. Wohn, and A. R. Smith, in Proceedings of the 7th High Energy Heavy Ion Study, Darmstadt, 1984, edited by R. Bock, H. H. Gutbrod, and R. Stock (GSI, Darmstadt, 1984), p. 753.
[7]Digital DATA Library, Photonuclear DATA CENTER, Office of Standard Reference DATA, National Bureau of Standards, Washington, D.C. 20234.
[8]J. D. Jackson, *Classical Electrodynamics* (Wiley, New York, 1975), 2nd ed., p. 719.
[9]R. Jäckle and H. Pilkuhn, Nucl. Phys. **A247**, 521 (1975).
[10]A. Goldberg, Nucl. Phys. **A240**, 636 (1984).
[11]A. Winther and K. Alder, Nucl. Phys. **A319**, 518 (1979).
[12]C. A. Bertulani and G. Baur, Nucl. Phys. **A442**, 739 (1985).
[13]A. R. Smith, J. B. McCaslin, J. V. Geaga, J. C. Hill, and J. P. Vary, Phys. Rev. C **28**, 1614 (1983).
[14]H. L. Anderson, D. A. Larson, L. C. Myrianthopoulos, L. Dubal, C. K. Hargrove, E. P. Hincks, R. J. McKee, H. Mes, D. Kessler, and A. C. Thompson, Phys. Rev. D **9**, 580 (1974).
[15]J. B. Cumming, G. Friedlander, and C. E. Swartz, Phys. Rev. **111**, 1386 (1958).
[16]J. B. Cumming, Annu. Rev. Nucl. Sci. **13**, 261 (1963).
[17]K. R. Hogstrom, Phys. Rev. **14**, 753 (1976).
[18]J. B. Cumming, V. Agoritsas, and R. Witkover, Nucl. Instrum. Methods **180**, 37 (1981).
[19]L. K. Peker, Nucl. Data Sheets **42**, 457 (1984).
[20]R. L. Bunting and J. J. Kraushaar, Nucl. Data Sheets **18**, 87 (1976).
[21]J. Halperin, Nucl. Data Sheets **28**, 485 (1979).
[22]S. B. Kaufman and E. P. Steinberg, Phys. Rev. C **22**, 167 (1980).
[23]A. S. Goldhaber and H. H. Heckman, Annu. Rev. Nucl. Part. Sci. **28**, 161 (1978); R. M. Raisbeck and F. Yiou, Phys. Rev. Lett. **35**, 155 (1975); D. L. Olsen, B. L. Berman, D. E. Greiner, H. H. Heckman, P. J. Lindstrom, and H. J. Crawford, Phys. Rev. C **28**, 1602 (1983).
[24]J. Benecke, T. T. Chou, C. N. Yang, and E. Yen, Phys. Rev. **188**, 2159 (1969).
[25]S. B. Kaufman, E. P. Steinberg, B. D. Wilkins, and D. J. Henderson, Phys. Rev. C **22**, 1897 (1980).
[26]G. D. Cole and N. T. Porile, Phys. Rev. C **24**, 2038 (1981).
[27]N. T. Porile, G. D. Cole, and C. R. Rudy, Phys. Rev. C **19**, 2288 (1979).
[28]J. B. Cumming, R. W. Stoenner, and P. E. Haustein, Phys. Rev. C **14**, 1554 (1976); J. B. Cumming, P. E. Haustein, T. J. Ruth, and G. J. Virtes, *ibid.* **17**, 1632 (1978).
[29]S. B. Kaufman, M. W. Weisfield, E. P. Steinberg, B. D. Wilkins, and D. Henderson, Phys. Rev. C **14**, 1121 (1976).
[30]B. C. Cook, private communication.
[31]J. P. Vary, private communication.
[32]R. J. Glauber, in *High Energy Physics and Nuclear Structure,* edited by G. Alexander (North-Holland, Amsterdam, 1967), p. 311; W. Czys and L. C. Maximon, Ann. Phys. (N.Y.) **52**, 59 (1969).
[33]S. Barshay, C. B. Dover, and J. P. Vary, Phys. Rev. C **11**, 360 (1975).
[34]N. R. Collard, L. R. B. Elton, and R. Hofstadter, in *Landolt-Börnstein: Numerical Data and Functional Relationships in Science and Technology,* edited by K.-H. Hellwege and H. Schopper (Springer, Berlin, 1967), Group I, Vol. 2, p. 21, and references therein.
[35]R. M. DeVries and H. G. Fischer, in *Quark Matter Formation and Heavy Ion Collisions,* edited by M. Jacob and H. Satz (World-Scientific, Singapore, 1982), p. 513.